

Distribution of Si II $\lambda 6355$ Velocities of Type Ia Supernovae and Implications for Asymmetric Explosions

Keto D. Zhang,^{1,2*} WeiKang Zheng,^{1†} Thomas de Jaeger,^{1,3} Benjamin E. Stahl,^{1,4,5}
Thomas G. Brink,¹ Xuhui Han,⁶ Daniel Kasen,^{1,4,7} Ken J. Shen,¹ Kevin Tang,¹
Alexei V. Filippenko^{1,8}

¹ Department of Astronomy, University of California, Berkeley, CA 94720-3411, USA.

² Google Lick Predoctoral Fellow.

³ Bengier Postdoctoral Fellow.

⁴ Department of Physics, University of California, Berkeley, CA 94720, USA.

⁵ Marc J. Staley Graduate Fellow.

⁶ Key Laboratory of Space Astronomy and Technology, National Astronomical Observatories, Chinese Academy of Sciences, Beijing 100101, China.

⁷ Lawrence Berkeley National Laboratory, Berkeley, CA, USA.

⁸ Miller Institute for Basic Research in Science, University of California, Berkeley, CA 94720, USA.

Accepted XXX. Received YYY; in original form ZZZ

ABSTRACT

The ejecta velocity is a very important parameter in studying the structure and properties of Type Ia supernovae (SNe Ia). It is also a candidate key parameter in improving the utility of SNe Ia for cosmological distance determinations. Here we study the velocity distribution of a sample of 311 SNe Ia from the kaepora database. The velocities are derived from the Si II $\lambda 6355$ absorption line in optical spectra measured at (or extrapolated to) the time of peak brightness. We statistically show that the observed velocity has a bimodal Gaussian distribution consisting of two groups of SNe Ia: Group I with a lower but narrower scatter ($\mu_1 = 11,000 \text{ km s}^{-1}$, $\sigma_1 = 700 \text{ km s}^{-1}$), and Group II with a higher but broader scatter ($\mu_2 = 12,300 \text{ km s}^{-1}$, $\sigma_2 = 1800 \text{ km s}^{-1}$). The population ratio of Group I to Group II is 201:110 (65%:35%). There is substantial degeneracy between the two groups, but for SNe Ia with velocity $v > 12,000 \text{ km s}^{-1}$, the distribution is dominated by Group II. The true origin of the two components is unknown, though there could be that naturally there exist two intrinsic velocity distributions as observed. However, we try to use asymmetric geometric models through statistical simulations to reproduce the observed distribution assuming all SNe Ia share the same intrinsic distribution. In the two cases we consider, 35% of SNe Ia are considered to be asymmetric in Case 1, and all SNe Ia are asymmetric in Case 2. Simulations for both cases can reproduce the observed velocity distribution but require a significantly large portion ($> 35\%$) of SNe Ia to be asymmetric. In addition, the Case 1 result is consistent with recent polarization observations that SNe Ia with higher Si II $\lambda 6355$ velocity tend to be more polarized.

Key words: supernovae: general — methods: statistical

1 INTRODUCTION

Type Ia supernovae (SNe Ia; see, e.g., Filippenko 1997 for a review of supernova classification) are the thermonuclear runaway explosions of carbon/oxygen white dwarfs (see, e.g., Hillebrandt & Niemeyer 2000; Howell 2011 for reviews). One of the most important applications of SNe Ia is that they can be used as standardisable

candles for measuring galaxy distances and thus the expansion history of the Universe (Riess et al. 1998; Perlmutter et al. 1999; Riess 2019).

There are two generally favoured progenitor systems for SNe Ia: the single-degenerate scenario (Whelan & Iben 1973), in which a single white dwarf accretes material from a nondegenerate companion star, and the double-degenerate scenario (Iben & Tutukov 1984; Webbink 1984) involving two white dwarfs. In the single-degenerate scenario, the nondegenerate companion star can survive after the SN ejecta collide with the companion star (Kasen 2010).

* E-mail: keto.zhang@gmail.com

† E-mail: weikang@berkeley.edu

In the double-degenerate scenario, various models predict different outcomes for the companion star. For example, in both the merger model (e.g., Pakmor et al. 2012) and the head-on collision model (e.g., Kushnir et al. 2013), the companion white dwarf is also destroyed. On the other hand, in some models the companion white dwarf could survive (e.g., Shen et al. 2018). A few SNe Ia with early-time observations have already ruled out a giant companion (e.g., Silverman et al. 2012c; Zheng et al. 2013; Goobar et al. 2014; Cao et al. 2015; Im et al. 2015; Hosseinzadeh et al. 2017; Holmbo et al. 2019; Li et al. 2019; Kawabata et al. 2019; Han et al. 2020), and for the extreme case of SN 2011fe, the companion was constrained to be a white dwarf (Nugent et al. 2011; Bloom et al. 2012), thus favoring the double-degenerate scenario. However, such early-time observations are still quite rare, and our understanding of the progenitor systems and explosion mechanisms remains substantially incomplete both theoretically and observationally (see a recent review by Jha et al. 2019).

Asymmetric ejecta of SNe Ia are also predicted by different models. While the single-degenerate model suggests that the ejecta can be quasispherical on large scales (e.g., Seitenzahl et al. 2013; Sim et al. 2013), in violent merger models the ejecta can depart from spherical symmetry on large angular scales (e.g., Pakmor et al. 2010; Moll et al. 2014; Raskin et al. 2014), thus resulting in different ejecta velocities seen from different viewing angles. The observed ejecta velocity is thus a very important parameter in studying the structure and properties of SNe Ia, and can also be used for improving the luminosity vs. light-curve shape relation used to standardise SNe Ia. For example, Foley & Kasen (2011), Wang et al. (2009, 2013), and Zheng et al. (2018) show that by classifying SNe Ia into subgroups according to their ejecta velocities, or directly adopting ejecta velocity as an additional parameter in the luminosity relation, one can reduce the scatter by 0.04–0.08 mag.

In this paper, we statistically study the distribution of Si II $\lambda 6355$ velocities measured at the time of peak brightness and use the velocity information as the only input data to explore the asymmetry of SNe Ia through statistical simulations.

2 DATA SELECTION

The velocity of the SN ejecta can be measured from the observed absorption minima in P-Cygni line profiles. The most prominent optical line in SNe Ia during the photospheric phase is Si II $\lambda 6355$, whose velocity is usually an indication of its photospheric velocity. Here we intend to study the Si II $\lambda 6355$ velocity distribution at peak brightness; ideally, it is best that a good spectrum be taken right at the time of peak brightness, but this is difficult to do in practice. In general, although the Si II $\lambda 6355$ velocity decreases dramatically as a power law during the first few days after explosion, it usually exhibits a slow (close to linear) decline around the time of peak brightness (e.g., Silverman et al. 2012b; Zheng et al. 2017; Stahl et al. 2020). Therefore, as long as there is a spectrum observed within a few days on either side of peak brightness (typically a 1-week interval), one can extrapolate the velocity to the time of peak brightness.

Several groups have already published many Si II $\lambda 6355$ velocities near the time of peak brightness (e.g., Foley et al. 2011; Wang et al. 2013; Folatelli et al. 2013; Zheng et al. 2018; Siebert et al. 2019). Among them, Siebert et al. (2019) released the largest number of appropriate SNe Ia (311 total) through the kaepora database

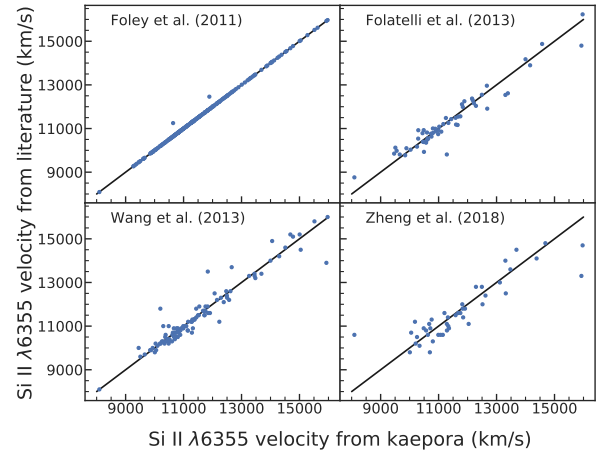


Figure 1. Comparison of Si II $\lambda 6355$ velocities of the overlapping SNe between the kaepora sample and the other four sources from the literature.

(v1.0)¹. This database is compiled from heterogeneous sources (see Siebert et al. 2019 and references therein for details), with the majority from the Center for Astrophysics Supernova Program (Blondin et al. 2012), the Berkeley SN Ia Program (Silverman et al. 2012a), and the Carnegie Supernova Project (Folatelli et al. 2013). It contains all the SNe Ia originally published by Foley et al. (2011), as well as dozens of new samples measured with the same methods as given by Foley et al. (2011).

In total, these datasets report the Si II $\lambda 6355$ velocity near the time of peak brightness for 395 SNe Ia. Note that each research group adopts a different method to measure the Si II $\lambda 6355$ velocity, so we compare their values. Since the kaepora database contains the largest sample, we compare other samples with that of kaepora and find an overlap of 272 objects; see Figure 1. Overall, the velocities are consistent with each other, but a few outliers are seen. To keep the measurements consistent, and also considering that the kaepora sample (311 SNe Ia) already includes most of the SNe Ia, we decided to only adopt the 311 objects in the kaepora sample in our analysis.

One concern about the data selection is potential bias. Here we select the SNe based on their spectral properties; specifically, at least one spectrum must be taken within a few days of peak brightness in order to derive the Si II $\lambda 6355$ velocity at the time of peak brightness through the relation of Foley et al. (2011) (see also Siebert et al. 2019). No other criteria, either the properties of the SN Ia itself (e.g., Δm_{15} , rise time) or the properties of its host galaxy (e.g., morphology, mass), are directly used to select the sample; therefore, those properties should not dominate the bias. However, since the SNe are discovered through photometry, if there is a correlation between the velocity and the peak luminosity, our sample could be biased. For example, if SNe with higher velocities are typically more luminous than lower-velocity SNe, high-velocity SNe are more likely to be discovered at larger redshifts than low-velocity SNe. To explore this potential bias, we divide our sample into two groups, one at low redshift and the other at high redshift, and perform Kolmogorov-Smirnov (KS) test on the two groups. Figure 2 (left panel) shows the histogram of all SNe Ia in our sample that have host-galaxy redshift information from the kaepora database (291 out of 311 objects in our sample). We set the break

¹ <https://msiebert1.github.io/kaepora/>

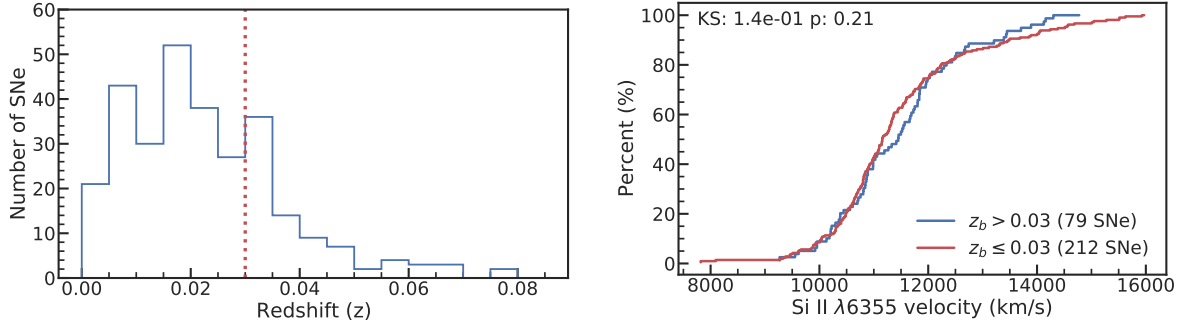


Figure 2. Left: Histogram of 291 SNe Ia (out of 311) from the kaepora sample that have host-galaxy redshift information, with $z = 0.03$ shown as a red dotted line. Right: The cumulative distribution of the 291 SNe Ia breaks into low- and high- redshift groups with $z_b = 0.03$. A KS test between the two groups gives a p -value of 0.21, indicating no significant difference between the two groups.

redshift to be $z_b = 0.01, 0.02, 0.03$ and 0.04 (note that both the mean and median redshifts are 0.02). Tests give KS values of 0.13, 0.15, 0.14, and 0.13, and (respectively) p -values of 0.37, 0.05, 0.21, and 0.71; Figure 2 (right panel) shows an example for $z_b = 0.03$. Our test demonstrates that except for $z_b = 0.02$, all other tests ($z_b = 0.01, 0.03$ and 0.04) did not exhibit a significant difference between the two groups. It is unknown why the KS test shows a significant difference between the two groups only at $z_b = 0.02$; so, in addition, we conducted a KS test with $z < 0.01$ (64 SNe) and $z > 0.04$ (30 SNe), giving a KS value of 0.16 and a p -value of 0.61, suggestive of insignificant differences. We thus conclude that there is no strong bias in our sample with SNe at low and high redshifts.

3 BIMODAL JUSTIFICATION

Wang et al. (2013) found that the distribution of Si II $\lambda 6355$ velocities near the time of peak brightness in SNe Ia shows a bimodal structure (see their Fig. 1c), with normal-velocity and high-velocity Gaussian components having respective peaks centred at $10,800 \text{ km s}^{-1}$ and $13,000 \text{ km s}^{-1}$ in the fit. While this bimodal structure is relatively obvious, they did not show the statistical improvement of the two-Gaussian fit over the one-Gaussian fit. Here we examine this issue with the above-selected sample of 311 SNe Ia, nearly doubling the number of objects (165 were used by Wang et al. 2013).

There are several methods for testing the significance in distributions, a popular one being the Pearson’s χ^2 statistic (not to be confused with reduced χ^2 statistics). Pearson’s χ^2 test can handle cases with counts that are dimensionless and have no meaningful uncertainties, as compared with those used in reduced χ^2 statistics where the errors come from the variance in each observation. A disadvantage of Pearson’s χ^2 method is that it depends on how one bins the data, and problems can be caused if the number of counts within some bins is small (e.g., Horváth 1998). However, another popular technique, the maximum-likelihood (ML) method (e.g., Horváth et al. 2008), is not sensitive to this problem because it treats each measurement independently. For our purposes, given that the observed Si II $\lambda 6355$ velocities could be rare at the high- or low-velocity ends (and thus the counts could be small within those bins), it is more appropriate to adopt the ML method.

3.1 Maximum-Likelihood Method

The ML method requires the assumption that each observation x comes from an underlying population distribution modeled as a probability density function $g(x, p_1, \dots, p_m)$, where p_1, \dots, p_m are parameters in the probability density function. Having N observations of x , we assume each observation x is independently sampled from identical distributions. Therefore, the chance of obtaining all N observations is given by the function called the likelihood function,

$$l = \prod_{i=1}^N g(x_i, p_1, \dots, p_m), \quad (1)$$

or in a more convenient logarithmic form called the log-likelihood,

$$L = \log l = \sum_{i=1}^N \log(g(x_i, p_1, \dots, p_m)). \quad (2)$$

The ML procedure maximises the log-likelihood L_{\max} for all possible values of the parameter p_1, \dots, p_m determined by some defined parameter space. Since the logarithmic function is monotonic, the log-likelihood function reaches maximum where the likelihood function does as well.

Since the likelihood is the chance of an observation under some hypothesis of the underlying population, if there are two hypotheses, the ratio of two likelihoods (called the likelihood ratio) states how likely one hypothesis is compared to the other. The likelihood ratio is better interpreted using the likelihood ratio χ^2 statistics (not to be confused with the Pearson’s χ^2 statistics as introduced in the previous section),

$$\chi^2 = 2(L_{1,\max} - L_{0,\max}), \quad (3)$$

where $L_{0,\max}$ and $L_{1,\max}$ are the log-likelihoods of the null hypothesis and alternative hypothesis, respectively. The likelihood ratio χ^2 statistics is asymptotically distributed as χ^2 with d degrees of freedom, which equals the difference in the number of free parameters between the alternative and null hypothesis.

3.2 Applying Maximum Likelihood to the Data

In our case, the observable variable x is the Si II $\lambda 6355$ velocity v . We take the hypothesis that v is distributed normally; more specif-

ically, it is distributed as the sum of k normal components, where the components have the functional form

$$f_l(v, \mu_l, \sigma_l) = \frac{1}{\sigma_l \sqrt{2\pi}} \exp\left(-\frac{(v - \mu_l)^2}{2\sigma_l^2}\right), \quad (4)$$

where μ_l and σ_l are respectively the mean and standard deviation (unknown parameters). We therefore have the probability density function

$$g(v_i, \mu_1, \sigma_1, \dots, \mu_k, \sigma_k) = \sum_{l=1}^k w_l f_l(v_i, \mu_l, \sigma_l), \quad (5)$$

where w_l is the weight for the l -th component (out of k components), and $\sum_{l=1}^k w_l = N$. The log-likelihood function is then composed of the logged sum across all probabilities for $N = 311$ SNe,

$$L_k = \sum_{i=1}^N \log\left(\sum_{l=1}^k w_l f_l(v_i, \mu_l, \sigma_l)\right). \quad (6)$$

To find the maximum of L_k , we adopt SciPy's implementation of Nelder-Mead optimisation, `scipy.optimize`², in Python 3 to determine the argmax simultaneously for each of the parameters μ_l , σ_l , and w_l . We start with only one normal component ($k = 1$) and find $L_{1,\max} = -2683$. We then add another normal component ($k = 2$) and find $L_{2,\max} = -2648$, statistically significantly higher than $L_{1,\max}$, which is a strong argument that two-component fitting is better than one-component fitting (see below for a more detailed discussion about the statistical improvement). We also try to adopt a third normal component, but the optimisation program was not able to converge and the resulting log-likelihood does not significantly differ from the results of using two components. This indicates that a third component is not needed for the fitting. We thus focus our discussion on the one- and two-component cases.

In Table 1, we list the best estimated parameters for the one- and two-component cases and plot the results in Figure 3. In the one-component case, we find best-estimated parameters of $\mu_1 = 11,500 \text{ km s}^{-1}$ and $\sigma_1 = 1300 \text{ km s}^{-1}$ with w_1 fixed to be 311 (shown as the black dotted line in Figure 3). The two-component case consists of a group of SNe Ia with a lower and narrower-scatter velocity ($\mu_1 = 11,000 \text{ km s}^{-1}$, $\sigma_1 = 700 \text{ km s}^{-1}$, and $w_1 = 201$, shown as a blue dot-dashed line in Figure 3), and another group of SNe Ia with a higher and broader-scatter velocity ($\mu_2 = 12,300 \text{ km s}^{-1}$, $\sigma_2 = 1800 \text{ km s}^{-1}$, and $w_2 = 110$, shown as a red dashed line in Figure 3). The combination of the two groups is illustrated with a black solid line in Figure 3. Our results are similar to those of Wang et al. (2013), who reported a lower velocity with $\mu_1 = 10,800 \text{ km s}^{-1}$ and a higher velocity with $\mu_2 = 13,000 \text{ km s}^{-1}$ (no scatter values were reported).

For comparison, we also use the least-squares binned fitting method scored by the Pearson's χ^2 statistic to fit the histogram distribution of Si II $\lambda 6355$ velocities with one and two normal components. The data are binned into 9 bins with width 500 km s^{-1} , where bin 1 is $v \leq 9500 \text{ km s}^{-1}$ and bin 9 is $v > 13,000 \text{ km s}^{-1}$. The bins were chosen purposefully so that each bin has at least an expected count of 4. The fitting results are also listed in Table 1; we see that the best-fit parameters from the χ^2 fitting are very close

to those of the ML method. For the two-components case, the χ^2 fitting also reveals that there is a lower velocity, narrower-scatter group and a higher velocity, broader scatter group, confirming the findings from the ML method. Note that since Pearson's χ^2 method has the disadvantage of depending on how one bins the data, we only adopt ML method result for further analysis.

3.3 Statistical Improvement

To estimate the statistical improvement of the two-component fitting over the one-component fitting, we first look at the likelihood ratio χ^2 statistics in the ML method according to Equation (3). We take the null hypothesis that the data are distributed as a unimodal normal $k = 1$. The alternative hypothesis adds a new component — that is, moving from $k = 1$ to $k = 2$, the ML solution of $L_{1,\max}$ changes to $L_{2,\max}$. This also increases the number of free parameters by 3 (w_2 , μ_2 , and σ_2). Applying Equation (3) to $L_{2,\max}$ and $L_{1,\max}$, we find that the likelihood ratio χ^2 statistic is 70 with 3 degrees of freedom. The p -value calculated from the χ^2 statistic is much less than 0.01; hence, the improvement of the two-component model over the one-component model is statistically significant.

As an independent check, we also adopt the Akaike Information Criterion (AIC; Akaike 1974) to apply a penalty according to the number of free parameters to prevent overfitting. The AIC makes it possible to perform model selection when the models have different numbers of free parameters. To be sensitive to the sampling error of a small dataset, we use the modified version of AIC denoted as AICc (Sugiura 1978),

$$\text{AICc} = -2L_{\max} + 2d + \frac{2d(d+1)}{N-d-1} \quad (7)$$

where d is the number of parameters and N is the sample size. A difference of 2 in the AICc provides positive evidence for the model having higher AICc, while a difference of 6 offers strong positive evidence (e.g., Kass & Raftery 1995; Mukherjee et al. 1998). We use the L_{\max} from the likelihood fitting method given in Table 1. For $k = 1$ and $k = 2$, we calculate AICc = 5360 and 5285, respectively; thus, from one component ($k = 1$) to two components ($k = 2$), the change in AICc is 75 (much greater than 6), which gives strong positive evidence that $k = 2$ produces a better fit than $k = 1$.

In conclusion, both the likelihood ratio test and the AICc test show strong statistical improvements for $k = 2$ fitting than $k = 1$ fitting. Therefore, if the velocity distribution is distributed normally (i.e., Gaussian mixture models), then the observed velocity is best described as two independent Gaussian distributions (Group I and Group II): one group with lower, narrower-scatter velocity ($\mu_1 = 11,000 \text{ km s}^{-1}$, $\sigma_1 = 700 \text{ km s}^{-1}$) and another group with higher, broader-scatter velocity ($\mu_2 = 12,300 \text{ km s}^{-1}$, $\sigma_2 = 1800 \text{ km s}^{-1}$). The ratio of the two groups is 201:110 (corresponding to 65%:35%) in the number of samples from the weight parameters. This velocity distribution is henceforth called the bimodal Gaussian distribution.

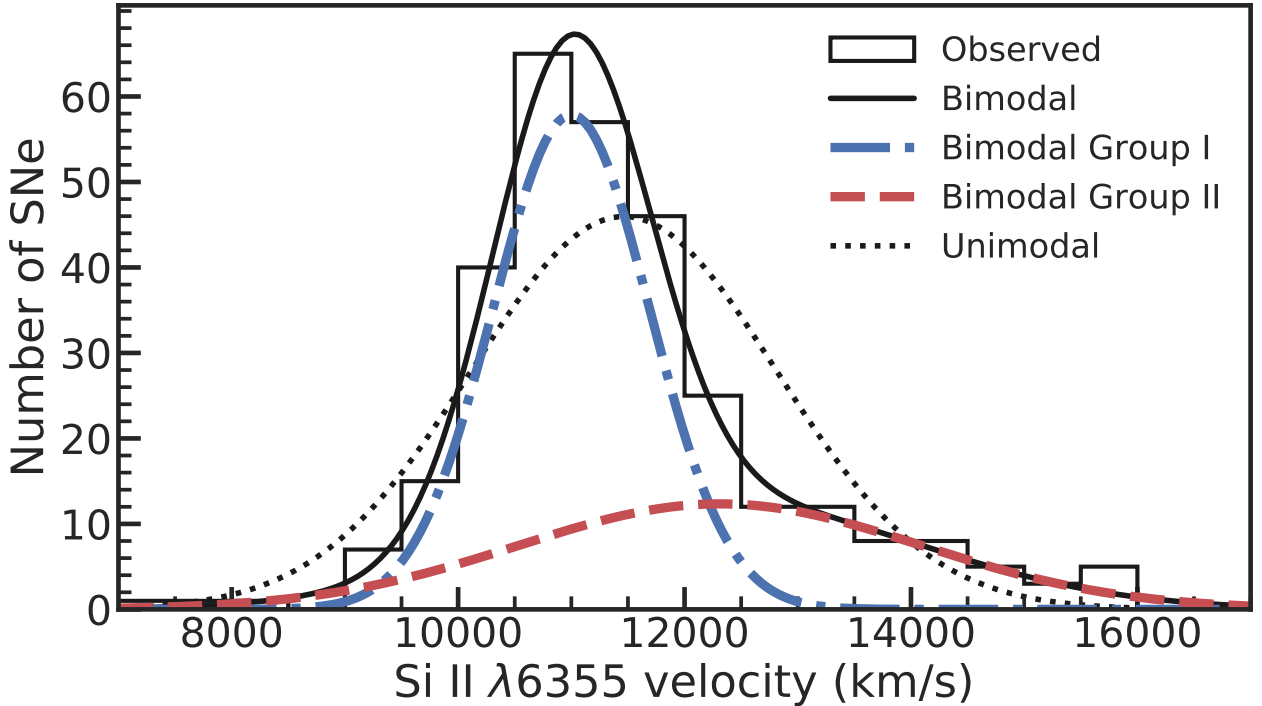
As one can see from Figure 3 for the two-component result, the second group of SNe Ia, whose mean velocity is higher than that of the first group, also has greater scatter than the first group, so there is a large overlap with the first group on the low-velocity side (the high-velocity side is dominated by the second group). In fact, the low-velocity side from the second group extends even farther than the first group. We thus think it is inappropriate to name the first group as low-velocity SNe Ia and the second group as high-velocity SNe Ia. Instead, here we suggest naming the lower mean velocity group as “Group I” and the other group as “Group II.”

² <https://docs.scipy.org/doc/scipy/reference/optimize.html>

Table 1. Best Parameters from ML and χ^2 Fitting Methods

ML method	L_{\max}	w_1	μ_1 (km/s)	σ_1 (km/s)	w_2	μ_2 (km/s)	σ_2 (km/s)
$k = 1$	-2682	311	11,500	1300			
$k = 2$	-2647	201	11,000	700	110	12,300	1800

χ^2 method	χ^2/dof	w_1	μ_1 (km/s)	σ_1 (km/s)	w_2	μ_2 (km/s)	σ_2 (km/s)
$k = 1$	18.7/8	311	11,100	1000			
$k = 2$	9.44/5	236	11,000	800	75	13,200	1400

**Figure 3.** Histogram of the Si II $\lambda 6355$ velocity distribution of 311 SNe Ia from the kaepora sample. Black solid line is the bimodal fit from the ML method, and black dotted line is the unimodal fit with parameters described in Table 1. The bimodal fit consists of two components: Group I SNe Ia with lower and narrower-scatter velocity, $\mu_1 = 11,000 \text{ km s}^{-1}$ and $\sigma_1 = 700 \text{ km s}^{-1}$ (blue dot-dashed line), and Group II SNe Ia with higher and broader-scatter velocity, $\mu_2 = 12,300 \text{ km s}^{-1}$ and $\sigma_2 = 1800 \text{ km s}^{-1}$ (red dashed line).

Because of the large overlap between the two groups, it is difficult to assign a specific SN Ia with a given velocity to a specific group, especially if the velocity is in the range 9500 km s^{-1} to $12,000 \text{ km s}^{-1}$. But for a velocity beyond that range, one can compare the probability between the two groups according to the probability distribution function assuming the Si II $\lambda 6355$ velocity data came from independently sampling each (but be cautious because the observed SN counts in those ranges are small). For $v < 9500 \text{ km s}^{-1}$, the probability ratio between Group I and Group II is 21%:79%; for $v > 12,000 \text{ km s}^{-1}$, the ratio is 12%:88%. Furthermore, for $v > 13,000 \text{ km s}^{-1}$, the probability for being in Group II is $> 99\%$, which means almost all SNe Ia with velocity $> 13,000 \text{ km s}^{-1}$ belong to Group II according to the fitting.

4 STATISTICAL SIMULATION OF THE VELOCITY DISTRIBUTION

As we demonstrated above, it is almost certain that SN Ia ejecta velocities exhibit a bimodal Gaussian distribution: Group I with lower and narrower-scatter velocities and Group II with higher and broader-scatter velocities. Some recent studies show that these two groups have different properties. For example, polarization observations reveal that the high-velocity SNe Ia (belonging to Group II) tend to have larger line polarizations (Maund et al. 2010; Cikota et al. 2019). Wang et al. (2013) found that high-velocity SNe Ia are substantially more concentrated in the inner and brighter regions of their host galaxies. Wang et al. (2019) also found that high-velocity SNe Ia tend to have cold, dusty circumstellar material around their progenitors, based on the variable Na I D absorption and flattening of the B -band light curve starting 40 d after maximum light. Zheng

et al. (2018) found that high-velocity SNe Ia are generally not good standardisable candles. Furthermore, Polin et al. (2019) proposed a model for a subclass of SNe Ia from sub-Chandrasekhar-mass progenitors with thin helium shells, and use the data from Zheng et al. (2018) to show that this model could be consistent with Group II SNe Ia.

While the true origin of the two components remains unknown, one simple explanation could be that there exist two intrinsic velocity distributions as we observed. However, here we focus on exploring another possibility, asymmetric geometry. We assume that all SNe Ia share the same intrinsic velocity distributions and test whether the observed bimodal velocity distributions could be caused by asymmetry for some SNe Ia. Our goal is to use asymmetric geometric models through statistical simulations to see whether the velocity distribution of Group II SNe Ia could be caused by angular geometry effects (i.e., ejecta-velocity variations at different viewing angles). Such asymmetries could be produced by various explosion models, such as delayed-detonation (e.g., Seitenzahl et al. 2013; Sim et al. 2013), detonation from failed deflagration (e.g., Kasen & Plewa 2007), double detonation (e.g., Townsley et al. 2019), violent white dwarf mergers (e.g., Pakmor et al. 2010; Moll et al. 2014; Raskin et al. 2014), and others (e.g., Kasen & Woosley 2009). The ejecta velocities measured from different viewing angles could differ by up to 4000 km s^{-1} (e.g., Kasen & Plewa 2007; Kasen & Woosley 2009; Townsley et al. 2019; Levanon & Soker 2019).

4.1 Two Asymmetric Models

Before starting the simulation of the velocity distributions, we need to quantify the velocity changes as a function of the viewing angle due to the asymmetric ejecta. To do this, we use the model spectra synthesised at different viewing angles to measure the Si II $\lambda 6355$ velocity. We adopt the synthesised spectra from two different models, one from Kasen & Plewa (2007) and the other from Townsley et al. (2019); these models provide spectra at the time of SN Ia peak brightness for different viewing angles. Note, however, that our simulation setups can be updated easily to adopt other models, if desired.

Kasen & Plewa (2007) studied in detail one model called Y12, selected from the detonating failed deflagration (DFD) scenario (Plewa 2007), which considers an off-center, mild ignition process in a degenerate Chandrasekhar-mass C-O white dwarf. In the Y12 model, the white dwarf is initially ignited within a small spherical region on the axis of symmetry, 50 km in size and offset 12.5 km from the center. A temporal series of synthetic spectra was calculated for different viewing angles; of particular interest to us are the spectra near the time of maximum brightness (see Fig. 7 of Kasen & Plewa 2007). In this model, the viewing angle was defined as $\theta = 0^\circ$ on the ignition side and $\theta = 180^\circ$ on the detonation side. We measure the Si II $\lambda 6355$ velocity from the maximum-light synthetic spectra at different viewing angles (simply treating them as real spectra) and plot the results in Figure 4, shown as blue circles.

Townsley et al. (2019) considered a double detonation that ignites first in a helium shell on the surface of the white dwarf; the He shell is heated by a directly impacting accretion stream and mixes modestly with the outer edge of the core. They use a white dwarf with a $1.0 M_\odot$ C-O core and a surface He layer with base $\rho = 2 \times 10^5 \text{ g cm}^{-3}$ and $T = 5 \times 10^8 \text{ K}$, having a mass of $0.021 M_\odot$. The He detonation is ignited with a spherical hotspot placed on the symmetry axis at the base of the He layer. Maximum-light spectra are synthesised at different averaged viewing angles

(see 4 of Townsley et al. 2019). Again, we measure the Si II $\lambda 6355$ velocity and plot the results in Figure 4, shown as red circles.

One can see that both models give very similar behavior for the Si II $\lambda 6355$ velocity as a function of viewing angle: the highest velocity appears at $\theta = 0^\circ$. The velocity decreases linearly as the viewing angle increases (toward the detonation side). But after θ around 100° , near the equator, the velocity becomes constant with almost no changes. To mathematically quantify this evolution, we use the following monotonically decreasing function to describe the data:

$$v = \begin{cases} v_c + \frac{\theta_c - \theta}{\theta_c} \Delta v & \theta \leq \theta_c \\ v_c & \theta > \theta_c, \end{cases} \quad (8)$$

where θ_c is the cutoff viewing angle, v_c is the constant velocity after the cutoff viewing angle, and Δv is the velocity difference between the cutoff velocity (where $\theta = 0^\circ$) and v_c . We use this function to fit the data from both models and plot the results in Figure 4. We find $\theta_c = (100 \pm 8)^\circ$, $v_c = (11.700 \pm 200.000) \text{ km s}^{-1}$, and $\Delta v = (5700 \pm 990) \text{ km s}^{-1}$ for the Kasen & Plewa (2007) model, and $\theta_c = (98 \pm 4)^\circ$, $v_c = (11.100 \pm 110.000) \text{ km s}^{-1}$, and $\Delta v = (5200 \pm 430) \text{ km s}^{-1}$ for the Townsley et al. (2019) model. The values for these parameters are very close to each other among the two models. Because of this, we will adopt only θ_c , v_c , and Δv as a single set of free parameters to be determined by the statistical simulation best fitted to the data as described in Section 4.2.

4.2 Simulation Setups

To simulate the distribution of velocities, we generate a sample size of $N = 10,000$ SN Ia cutoff velocities v_c individually sampled from the Group I Gaussian distribution, henceforth calling this sample the intrinsic distribution, which is also the input distribution for our simulation. We then consider the asymmetry effect according to the different parameters, applying it to a certain fraction of the SNe Ia (see details below); thus, the asymmetry-corrected velocity distribution, which is also the output sample from our simulation, changes from the intrinsic (input) distribution. We finally compare the asymmetry-corrected (output) velocity distribution with the observed distribution by adopting the KS test in order to find the best parameters. We define the parameter space from a grid search allowing the parameters to be within their respective ranges: $\theta_c \in \{0^\circ, 1^\circ, 2^\circ, \dots, 180^\circ\}$ with an increment of 1° , and $\Delta v \in \{3000, 3100, 3200, \dots, 7500\} \text{ km s}^{-1}$ with an increment of 100 km s^{-1} , giving a space of size 8280 pairs of parameters. The parameters are ranked by the KS values, and we select the top four best parameters for further discussion from the total of 8280 pairs of parameters. The simulation codes are written in Python 3 and can be found online.³

4.3 Results

We consider two cases for the asymmetry effect in our simulation: (1) only a portion of the SNe Ia from the intrinsic distribution are asymmetric, and (2) all of the SNe Ia from the intrinsic distribution are asymmetric.

For Case 1, considering the mean and scatter parameters of the two groups, it is natural to assume that Group I SNe Ia are symmetric

³ https://github.com/ketozhang/ejecta_velocities_of_type-Ia_supernovae

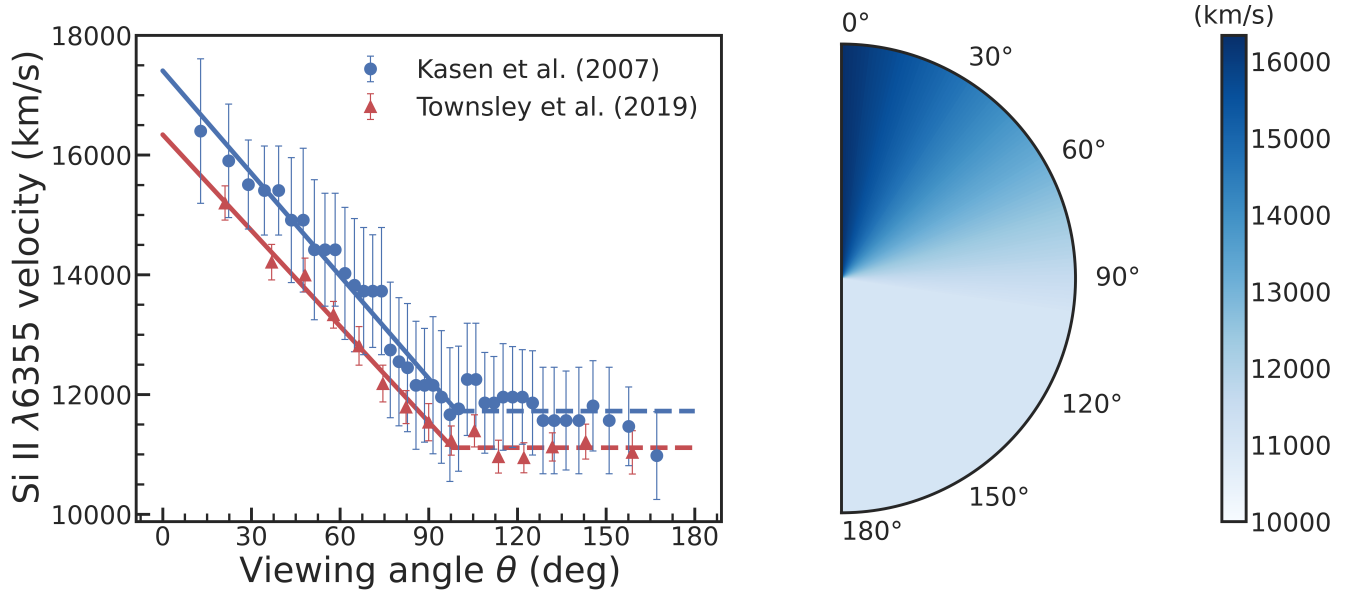


Figure 4. Left: Si II $\lambda 6355$ velocity (measured from the maximum-light synthetic spectra) as a function of viewing angle from the Kasen & Plewa (2007) and Townsley et al. (2019) models. The data are fitted with a monotonically decreasing function as described in the text. Right: Demonstration of the ejecta seen at different viewing angles which are color coded for the different velocities.

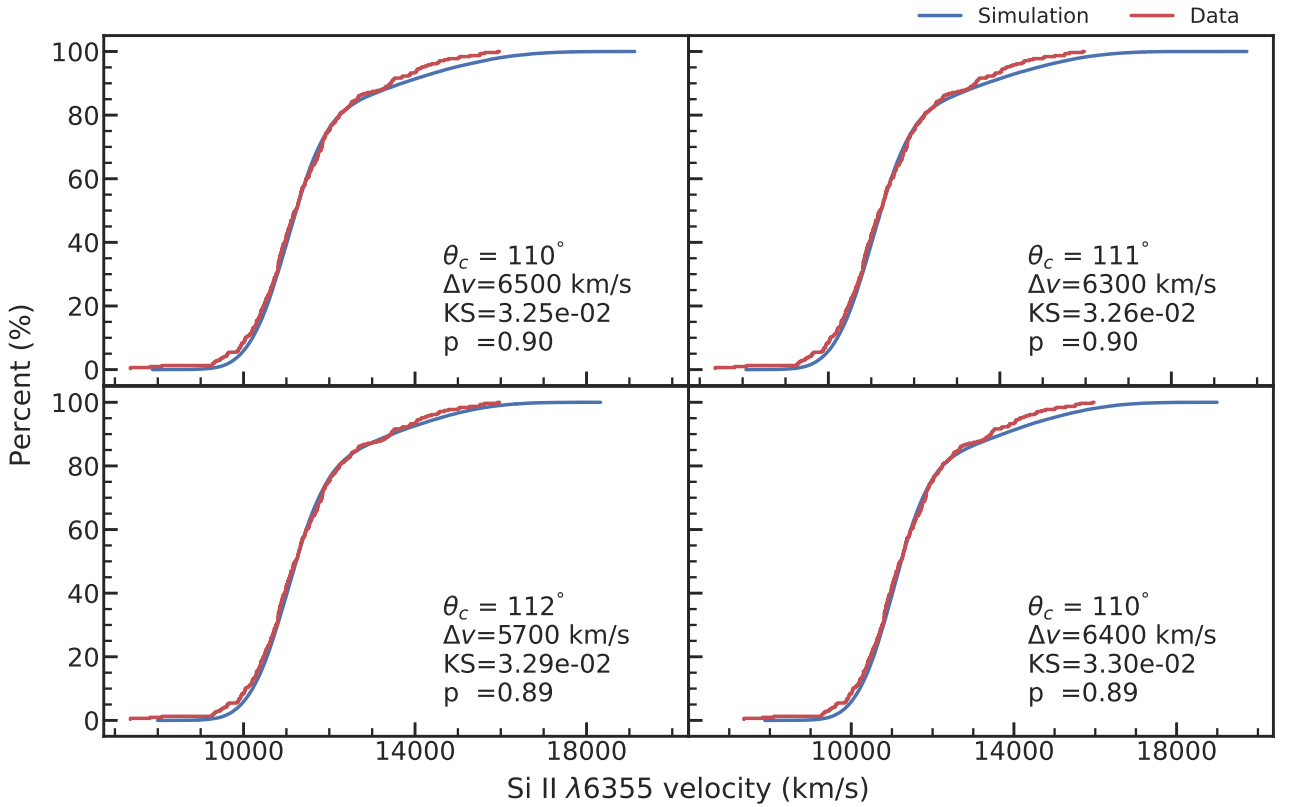


Figure 5. Cumulative distributions of the top four best-performing simulations (selected by the KS statistic) for Case 1, where a portion (35%) of all SNe Ia are assumed to be asymmetric in the simulation. These four simulations (blue) can reproduce the observed (red) velocity distribution.

while Group II SNe Ia are asymmetric, and we therefore assume 35% of the intrinsic distribution (namely the total number of Group II SNe Ia) need to be corrected for asymmetry from the intrinsic (input) distribution. To do this, we first generate $N = 10^5$ SN Ia velocities sampled from a Gaussian distribution with parameters taken from Group I SNe Ia ($\mu = 11,000 \text{ km s}^{-1}$ and $\sigma = 700 \text{ km s}^{-1}$). 64.6% of these SNe Ia (namely the total number in Group I) are unmodified and passed onto the final output result. For the remaining 35% of SNe Ia, being Group II, we treat them by applying the asymmetry model (Eq. 8), where v_c is taken from the generated velocities of the intrinsic distribution (i.e., v_c is sampled from the Group I Gaussian distribution), while θ_c and Δv are taken from the parameter space. The asymmetry-corrected (output) velocity for the final result is then calculated assuming the SN is equally observable in each unit solid angle. We achieve this by applying the spherical point-picking correction to the viewing angle $\theta = \arccos(2u - 1)$, where u samples the uniform(0, 1) distribution. We finally compare the asymmetry-corrected velocity distribution for all 10^5 SNe Ia with the observed distribution of 311 SNe Ia by adopting the KS test. This step is repeated for a total of 8280 sets of parameters θ_c and Δv in the parameter space.

Here we show the top four performing parameter sets in the KS test, as plotted in Figure 5. The KS statistic computes a distance between the empirical distribution of the simulation of 10^5 SNe Ia and the observed sample of 311 SNe Ia. The p -value is two-tailed, generated from the KS statistic and the null hypothesis that the two distributions come from the same population distribution. For reference, the KS statistic with the naive hypothesis that the underlying distribution is Gaussian with Group I parameters tested with the observed data produces a KS value of 0.19 and a p -value of 6.43×10^{-10} ; hence, we strongly reject the hypothesis that the observed data are normally distributed with Group I parameters. For the top four performing results shown in Figure 5, with an α level of 5%, the null hypothesis cannot be rejected. The best parameters out of the top four cases are $\theta_c = 111^\circ$ and $\Delta v = 6000 \text{ km s}^{-1}$ with a KS value of 3.2×10^{-2} and a p -value of 0.91. All four top cases have very similar best parameters, with θ_c in the range 110° to 112° and Δv of 5900 km s^{-1} to 6300 km s^{-1} . These parameters are very close to the values from the two asymmetric models given in Section 4.1. To produce confidence intervals, we create a joint probability space where the values are the parameters and the chance to observe the parameters is the p -value normalised by dividing the p -value with the sum of all 8280 p -values from the simulations. This probability space is then sampled 10,000 times to get a parameter distribution where the mean and standard deviation are used for the 1σ confidence interval. Doing so, the 1σ confidence interval is $\theta_c = (120 \pm 15)^\circ$ and $\Delta v = (5400 \pm 1200) \text{ km s}^{-1}$ at 1σ confidence.

For Case 2, instead of applying the asymmetric model to a subset of the intrinsic (input) distribution, we apply the asymmetric model to all $N = 10,000$ simulated SNe Ia from the intrinsic (input) distribution. Thus, we assume that all SNe Ia are asymmetric. The remaining simulation procedures follow exactly as in the Case 1. Similarly, we show the top four performing results in Figure 6. At an α level of 5%, the null hypothesis for all four top cases cannot be rejected, the same as in Case 1. The best parameters out of the top four simulations are $\theta_c = 60^\circ$ and $\Delta v = 6400 \text{ km s}^{-1}$, with a KS value of 3.3×10^{-2} and a p -value of 0.89. The 1σ confidence interval is calculated to be $\theta_c = (63 \pm 6)^\circ$ and $\Delta v = (5700 \pm 1100) \text{ km s}^{-1}$. Compared to Case 1, the obvious difference is in θ_c : for Case 2, θ_c is around 63° , which is much smaller than

in Case 1 ($\theta_c \approx 120^\circ$). The other parameter, Δv , is almost the same as for Case 1.

For both cases, at an α level of 5%, the null hypothesis for all four top simulations cannot be rejected, which indicates that for both cases, the simulations can reproduce the observed Si II $\lambda 6355$ velocity distribution. Also, while comparing to the models, both cases give a cutoff velocity Δv around 5500 km s^{-1} , matching well to the two models (5200 km s^{-1} and 5700 km s^{-1}). However, for the other parameter, the cutoff angle θ_c , Case 1 is apparently better than Case 2. The θ_c parameter from both models is $\sim 100^\circ$. From Case 1, θ_c is $\sim 120^\circ$, slightly larger, but much closer to 100° compared to Case 2, for which θ_c is $\sim 63^\circ$. For this reason, we favor Case 1 over Case 2.

As shown above, our simulations indicate that assuming a portion of SNe Ia are asymmetric, we can reproduce the observed Si II $\lambda 6355$ velocity distribution (Case 1). The asymmetric SNe Ia could occupy a notable fraction (35%) of the total SNe Ia. In fact, since the θ_c value in Case 1 ($120 \pm 15^\circ$) is slightly larger than in the model ($\sim 100^\circ$), while increasing the fraction of asymmetric SNe Ia in the simulation would reduce the θ_c value, a larger fraction of asymmetric SNe Ia would provide a better match between the simulation θ_c and the model; therefore our simulation indicates that more than 35% of SNe Ia are asymmetric. Note that for both cases, since the input distribution is the same for all SNe, all SNe Ia share the same intrinsic velocity distribution in our simulation. Even for Case 1, where 35% are asymmetric, all SNe Ia still share the same input distribution. The only difference is that the output distribution for the 35% SNe Ia are asymmetry-corrected. We therefore conclude that more than 35% of SNe Ia are asymmetric from our simulation if all SNe Ia share the same intrinsic velocity distribution based on the adopted models and simulations.

5 CONCLUSIONS AND DISCUSSION

We have studied the ejecta velocity distribution of a sample of 311 SNe Ia derived from the Si II $\lambda 6355$ absorption line measured at the time of peak brightness. We statistically show that the bimodal Gaussian yields the best fit in maximum likelihood to the observed velocity distribution, significantly better than one-Gaussian fitting. The bimodality suggests two velocity groups among SNe Ia: Group I with a lower velocity but narrow scatter ($\mu_1 = 11,000 \text{ km s}^{-1}$, $\sigma_1 = 700 \text{ km s}^{-1}$), and Group II with a higher velocity but broader scatter ($\mu_2 = 12,300 \text{ km s}^{-1}$, $\sigma_2 = 1800 \text{ km s}^{-1}$). The number ratio of the two groups is 201:110 (65%:35%) in our sample. There is substantial degeneracy between the two groups for SNe Ia with ejecta velocity below $12,000 \text{ km s}^{-1}$. However, for SNe Ia with velocity exceeding this value, the distribution is dominated by Group II (with a probability of 12%:88% between Group I and Group II), and almost all SNe Ia with velocity $> 13,000 \text{ km s}^{-1}$ belong to Group II (the probability of being in Group II is $> 99\%$).

Although the true origin of the two components is unknown, one simple explanation could be that naturally there exist two intrinsic velocity distributions as observed. However, we try to use asymmetric geometric models through statistical simulations to reproduce the observed velocity distributions assuming all SNe Ia originate from the same intrinsic (input) distribution. Specifically, we adopt a geometric model in which the velocity decreases linearly as the viewing angle θ increases, but then becomes constant after a certain cutoff θ_c . The velocity difference between $\theta = 0^\circ$ and θ_c gives another Δv parameter in our simulation. A total of 8280 pairs of θ and Δv are set up in our simulation. For each

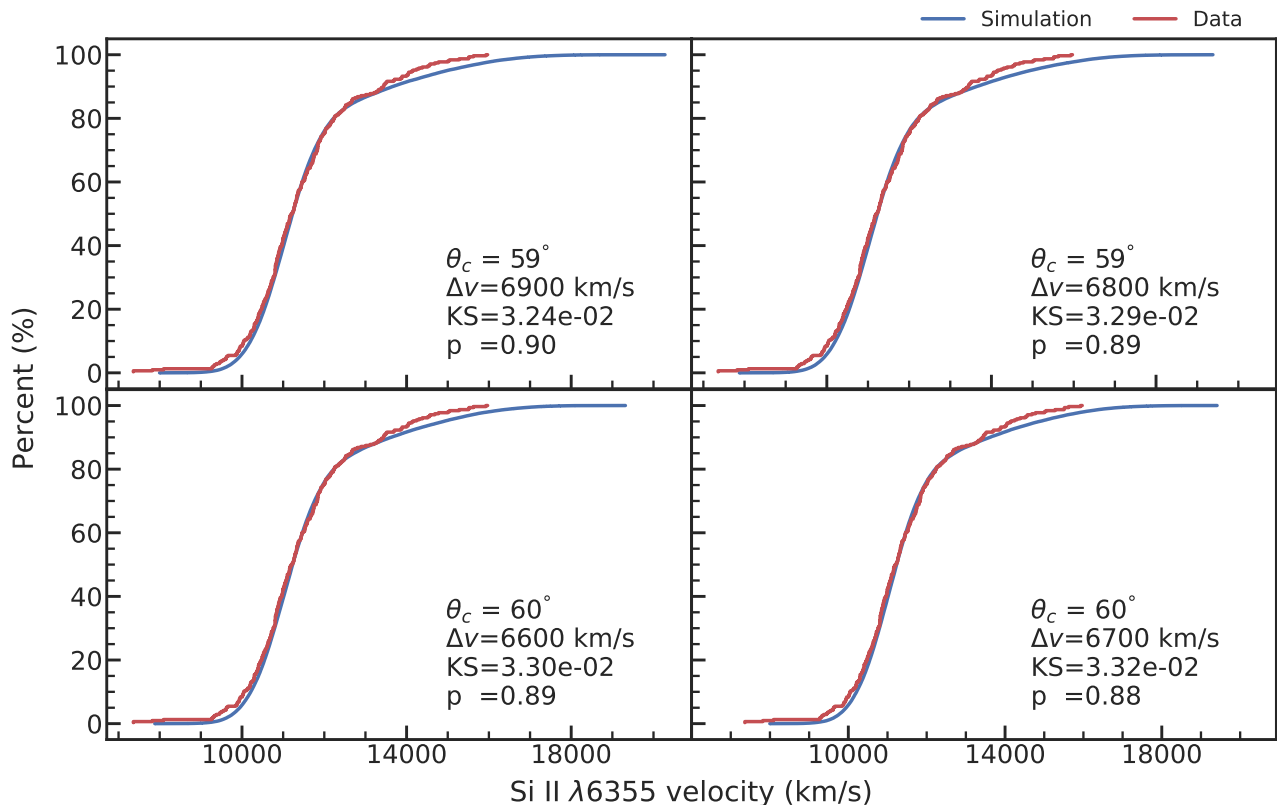


Figure 6. Same as Figure 5 but for Case 2, where all of the SNe Ia are assumed to be asymmetric in the simulation. These top four cases also can reproduce the observed (red) velocity distribution. Compared to Case 1, the obvious difference is the θ_c parameter, which decreased substantially.

pair, we generate a sample size of $N = 10^5$ velocities from the assumed intrinsic Gaussian distribution, and then we apply the geometric models to a certain fraction of them. We finally compare the asymmetry-corrected velocity (output) distribution with the observed distribution by adopting the KS test to find the best values of θ and Δv .

We considered two cases in our simulation. In Case 1, where only a portion (35%) of all SNe Ia are asymmetric, our simulation yields best-fit parameters $\theta_c = (120 \pm 15)^\circ$ and $\Delta v = (5400 \pm 1200) \text{ km s}^{-1}$. In Case 2, where all SNe Ia are asymmetric, our simulation yields best-fit parameters $\theta_c = (63 \pm 6)^\circ$ and $\Delta v = (5700 \pm 1100) \text{ km s}^{-1}$. We find that for both cases, the simulations can reproduce the observed Si II $\lambda 6355$ velocity distribution, giving a cutoff velocity $\Delta v \approx 5500 \text{ km s}^{-1}$, matching the models well. However, considering the other parameter (the cutoff angle θ_c), Case 1 ($120 \pm 15)^\circ$ is better than Case 2 ($63 \pm 6)^\circ$ compared with the models ($\sim 100^\circ$), so we favor Case 1. Regardless, we find that a significantly large portion ($>35\%$) of SNe Ia are asymmetric in our simulations, assuming all SNe Ia originate from the same explosion mechanism.

Observationally, spectropolarimetry provides an effective way to explore the geometry of SNe Ia (see Wang & Wheeler 2008 for a review). Interestingly, recent observations show that the Si II $\lambda 6355$ line polarization is correlated with the velocity of that line (Maud et al. 2010; Cikota et al. 2019): SNe Ia with higher Si II $\lambda 6355$ velocity tend to have stronger polarization. This correlation is consistent with our simulation Case 1, that a portion (35%) of all SNe Ia are asymmetric (and thus should have higher polarization), resulting

in Group II SNe Ia with higher Si II $\lambda 6355$ velocity on average. This provides another indication that simulation Case 1 is more favoured over Case 2. However, although our simulations show that a large portion of SNe Ia are asymmetric, many models can result in asymmetric explosions, so we are unable to distinguish which model is more favoured. Additional observations are required to explore more specific explosion models. For example, using high-quality nebular spectra of SNe Ia, Dong et al. (2015) discovered clear double-peaked line profiles in 3 out of ~ 20 SNe Ia, which is naturally expected from the direct white dwarf collision model (e.g., Kushnir et al. 2013), or the violent merger model when the companion is completely disrupted (e.g., Pakmor et al. 2012).

We therefore encourage more polarization and nebular observations of SNe Ia for further studies of asymmetries.

ACKNOWLEDGEMENTS

We thank the anonymous referee for useful comments. K.D.Z. was supported by the Anslem M&PS Fund through the Berkeley Summer Undergraduate Research Fellowship (SURF) program in 2019. A.V.F.'s group at U.C. Berkeley is grateful for financial assistance from Gary & Cynthia Bengier (T.de J. is a Bengier Postdoctoral Fellow), Marc J. Staley (B.E.S. is a Marc J. Staley Graduate Fellow), the Christopher R. Redlich Fund, the TABASGO Foundation, and the Miller Institute for Basic Research in Science (U.C. Berkeley). Research at Lick Observatory (where many of the SN Ia spectra

used here were obtained) is partially supported by a generous gift from Google, and K.D.Z. is a Google Lick Predoctoral Fellow.

6 DATA AVAILABILITY

The data and results underlying this article are available in Zenodo at <https://zenodo.org/record/4032100>.

REFERENCES

- Akaike H., 1974, *IEEE Transactions on Automatic Control*, **19**, 716
- Blondin S., et al., 2012, *AJ*, **143**, 126
- Bloom J. S., et al., 2012, *ApJ*, **744**, L17
- Cao Y., et al., 2015, *Nature*, **521**, 328
- Cikota A., et al., 2019, *MNRAS*, **490**, 578
- Dong S., Katz B., Kushnir D., Prieto J. L., 2015, *MNRAS*, **454**, L61
- Filippenko A. V., 1997, *ARA&A*, **35**, 309
- Folatelli G., Morrell N., Phillips M. M., et al., 2013, *ApJ*, **773**, 53
- Foley R. J., Kasen D., 2011, *ApJ*, **729**, 55
- Foley R. J., Sanders N. E., Kirshner R. P., 2011, *ApJ*, **742**, 89
- Goobar A., et al., 2014, *ApJ*, **784**, L12
- Han X., et al., 2020, *ApJ*, **892**, 142
- Hillebrandt W., Niemeyer J. C., 2000, *ARA&A*, **38**, 191
- Holmbo S., et al., 2019, *A&A*, **627**, A174
- Horváth I., 1998, *ApJ*, **508**, 757
- Horváth I., Balázs L. G., Bagoly Z., Veres P., 2008, *A&A*, **489**, L1
- Hosseinzadeh G., et al., 2017, *ApJ*, **845**, L11
- Howell D. A., 2011, *Nature Communications*, **2**, 350
- Iben Jr. I., Tutukov A. V., 1984, *ApJS*, **54**, 335
- Im M., Choi C., Yoon S.-C., Kim J.-W., Ehgamberdiev S. A., Monard L. A. G., Sung H.-I., 2015, *ApJS*, **221**, 22
- Jha S. W., Maguire K., Sullivan M., 2019, *Nature Astronomy*, **3**, 706
- Kasen D., 2010, *ApJ*, **708**, 1025
- Kasen D., Plewa T., 2007, *ApJ*, **662**, 459
- Kasen D., Woosley S. E., 2009, *ApJ*, **703**, 2205
- Kass R. E., Raftery A. E., 1995, *Journal of the American Statistical Association*, **90**, 773
- Kawabata M., et al., 2019, arXiv e-prints, p. arXiv:1908.03001
- Kushnir D., Katz B., Dong S., Livne E., Fernández R., 2013, *ApJ*, **778**, L37
- Levanon N., Soker N., 2019, *MNRAS*, **486**, 5528
- Li W., et al., 2019, *ApJ*, **870**, 12
- Maund J. R., et al., 2010, *ApJ*, **725**, L167
- Moll R., Raskin C., Kasen D., Woosley S. E., 2014, *ApJ*, **785**, 105
- Mukherjee S., Feigelson E. D., Jogesh Babu G., Murtagh F., Fraley C., Raftery A., 1998, *ApJ*, **508**, 314
- Nugent P. E., et al., 2011, *Nature*, **480**, 344
- Pakmor R., Kromer M., Röpke F. K., Sim S. A., Ruiter A. J., Hillebrandt W., 2010, *Nature*, **463**, 61
- Pakmor R., Kromer M., Taubenberger S., Sim S. A., Röpke F. K., Hillebrandt W., 2012, *ApJ*, **747**, L10
- Perlmutter S., Aldering G., Goldhaber G., et al., 1999, *ApJ*, **517**, 565
- Plewa T., 2007, *ApJ*, **657**, 942
- Polin A., Nugent P., Kasen D., 2019, *ApJ*, **873**, 84
- Raskin C., Kasen D., Moll R., Schwab J., Woosley S., 2014, *ApJ*, **788**, 75
- Riess A. G., 2019, *Nature Reviews Physics*, **2**, 10
- Riess A. G., Filippenko A. V., Challis P., et al., 1998, *AJ*, **116**, 1009
- Seitzzahl I. R., et al., 2013, *MNRAS*, **429**, 1156
- Shen K. J., et al., 2018, *ApJ*, **865**, 15
- Siebert M. R., et al., 2019, *MNRAS*, **486**, 5785
- Silverman J. M., Foley R. J., Filippenko A. V., et al., 2012a, *MNRAS*, **425**, 1789
- Silverman J. M., Kong J. J., Filippenko A. V., 2012b, *MNRAS*, **425**, 1819
- Silverman J. M., et al., 2012c, *ApJ*, **756**, L7
- Sim S. A., et al., 2013, *MNRAS*, **436**, 333
- Stahl B. E., et al., 2020, *MNRAS*, **492**, 4325

- Sugiura N., 1978, *Communications in Statistics - Theory and Methods*, **7**, 13
- Townsend D. M., Miles B. J., Shen K. J., Kasen D., 2019, *ApJ*, **878**, L38
- Wang L., Wheeler J. C., 2008, *ARA&A*, **46**, 433
- Wang X., et al., 2009, *ApJ*, **699**, L139
- Wang X., Wang L., Filippenko A. V., Zhang T., Zhao X., 2013, *Science*, **340**, 170
- Wang X., Chen J., Wang L., Hu M., Xi G., Yang Y., Zhao X., Li W., 2019, *ApJ*, **882**, 120
- Webbink R. F., 1984, *ApJ*, **277**, 355
- Whelan J., Iben Jr. I., 1973, *ApJ*, **186**, 1007
- Zheng W., et al., 2013, *ApJ*, **778**, L15
- Zheng W., et al., 2017, *ApJ*, **841**, 64
- Zheng W., Kelly P. L., Filippenko A. V., 2018, *ApJ*, **858**, 104

This paper has been typeset from a \LaTeX file prepared by the author.